Research Report

First-principles Study of Gum-metal Alloys: Mechanism of Ideal Strength

Naoyuki Nagasako, Ryoji Asahi and Jürgen Hafner

Report received on Mar. 16, 2013

ABSTRACT We have studied Ti-based gum-metal alloys to understand their ideal strength behavior by the first-principles density functional theory. The approximant of the gum metal, G1-type Ti_3Nb model structure, is determined to be the most favorable one among the possible configurations of four Nb atoms and twelve Ti atoms in a 16-atoms supercell. The ideal tensile strength and the ideal shear strength of the G1 structure are found to be 2.4 GPa and 1.45-1.65 GPa, respectively, which are much lower than those for conventional body-centered cubic simple metals. This is because the elastic softening occurs when the valence electron numbers per atom is around 4.24 featuring the gum-metal composition. The predicted shear strength is very close to the experimentally measured strength of gum-metal nanopillars, 1.7 GPa. Thus, it is confirmed that gum metal should be deformed by near ideal strength.

KEYWORDS First-principles Calculation, Density Functional Theory, Elastic Constant, Ideal Strength, Phonon Dispersion, Stress-strain Curve

1. Introduction

A class of Ti-Nb-Ta-Zr-O body-centered cubic (β phase) alloys, the so-called gum metal, are known to display a low elastic modulus, high strength, high yield strain, a very good ductility, inver property and elinvar property.[1] To clarify an origin of the low Young's modulus, we calculated elastic constants of Ti-based binary alloys by the first-principles method and investigated relations between elastic constants and electronic structures of alloys. Consequently, vanishing of tetragonal elastic constant, $C'=(C_{11}-C_{12})/2$, results in the low Young's modulus.[2] In addition, it is also found that vanishing of C' is achieved by properly controlling composition of gum metal such that its valence electron concentration per atom becomes 4.24. Since the ideal shear strength τ_{max} of body-centered cubic (bcc) simple metals can be estimated empirically by a relation

$$\tau_{max} \cong 0.11 G_{111} = 0.11 \times \frac{3C_{44}(C_{11}-C_{12})}{C_{11}-C_{12}+4C_{44}}, \quad \cdots\cdots\cdots\cdots\cdots (1)$$

the vanishing of C' implies that the ideal strength in gum metal is expected to be small.

To explain above-mentioned properties of gum metal, we have proposed possibility of dislocation-free deformation mechanism, where gum metal is considered to be deformed by near ideal strength under the two conditions: (1) the ideal strength itself is significantly small and (2) there exists some kinds of obstacle which prevents moving of dislocations. To verify the mechanism, predicting the ideal strength theoretically without using empirical formula of Eq. 1 and comparing with experiment[3] are critical issues.

In our early study[2] based on the ultrasoft pseudopotential (USPP) method, we assumed $D0_3$-type Ti_3Nb (see **Fig. 1**(a)) as an approximant of gum metal since gum metal is composed mostly of Titanium and Niobium with a typical composition of gum metal of Ti-23Nb-0.7Ta-2Zr-1.2O in atomic %. Then, we performed calculations of the elastic constants not only for Ti_3Nb but also for $D0_3$-type Ti_3X, TiX_3 and B2-type TiX (X = V, Nb, Ta, Mo and W) to seek for an origin of the low Young's modulus from the microscopic point of view. As we mentioned above, it was confirmed that vanishing of tetragonal shear constant turned out to be crucial to display the low Young's modulus. Although our previous calculations based on the $D0_3$-type Ti-based alloys could clearly describe trends of the tetragonal elastic constants, new calculations with more accurate projector augmented wave (PAW) method revealed that $D0_3$-type Ti_3Nb are found to be elastically unstable.[4] Namely, it has a negative value of C_{44} as shown in **Fig. 2**, which means that $D0_3$-type structure model is not adequate approximant for gum metal.

Recently, Lazar et al.[4] have found a more reliable structure model, G1 structure as shown in Fig. 1(b), by searching the most stable structure among all possible configurations of four Nb atoms and twelve Ti atoms in a large 16-atom supercell which consists of 2 × 2 × 2 bcc cells. In the $D0_3$ structure, each Nb atom is isotropically arranged. In contrast, in the G1 structure, Nb atoms occupy the sites along the body-diagonal of a 2 × 2 × 2 bcc supercell with direct Nb-Nb neighbors.

In the present work, we have predicted the ideal tensile and shear strength with the G1 model structure as an approximant for gum metal by the first-principles density functional techniques. This article is organized as follows: Sec. 2 describes the computational methods. In sec. 3, we show the features of the structure model for Ti_3Nb and its elastic stability. Sec. 4 presents the phonon calculations of the G1-type Ti_3Nb. Sec. 5 reports our calculated results for the ideal tensile and shear strength. In sec. 6, we briefly explain key mechanisms to develop properties of gum metal. Finally, we summarize our study in sec. 7.

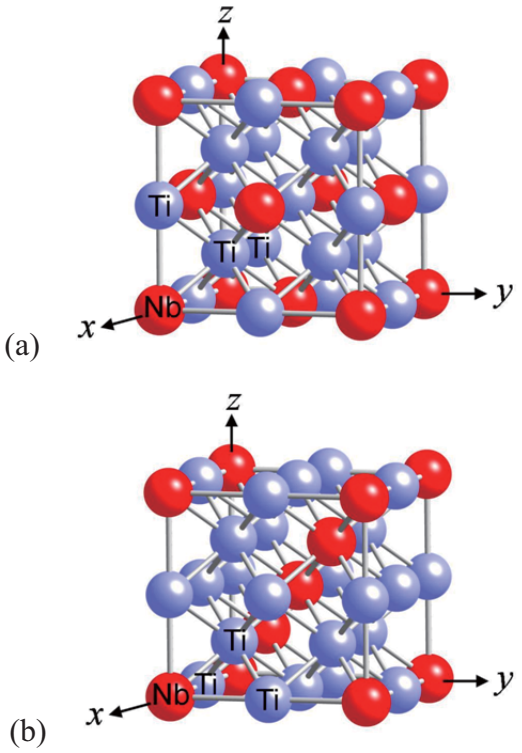

Fig. 1 Comparison of the $D0_3$ (a) and G1 (b) structures for a Ti_3Nb alloy. The atomic positions within the irreducible rhombohedral unit cell are labelled with the chemical symbols of the constituents. Ti atoms are shown in blue, Nb atoms in red.

2. Computational Methods

Calculations reported in our present study were performed with the PAW method[5,6] based on the generalized gradient approximation to density-functional theory as implemented in the Vienna ab-initio simulation package (VASP).[7,8] We assumed the exchange-correlation energy functional by Perdew et al.[9] The cutoff energy for the wave function is set to be 350 (eV).

The conventional phonon calculations at zero temperature were performed by the direct method, where dynamical matrix was constructed from the forces acting on the atoms displaced from their equilibrium positions. On the other hand, we also performed phonon calculations at finite temperature to discuss the dynamical stability of the G1-type Ti_3Nb. The phonon dispersion at finite temperatures were calculated by means of the self-consistent ab-initio lattice dynamical method (SCAILD) developed by Souvatzis et al.[10] In the SCAILD method, the improved phonon frequencies and atomic displacement vectors are estimated in a self-consistent manner from the results of phonon dispersion at previous step. The detail of the SCAILD method are described in the references.[11-14] Since the SCAILD method needs to re-calculate atomic forces at each iteration, a much larger computational effort is required than the conventional phonon calculations. Actually, we needed about 100 iterations to obtain fully converged phonon frequencies. The effects of thermal expansion and phonon damping were not taken into account in the present calculations because

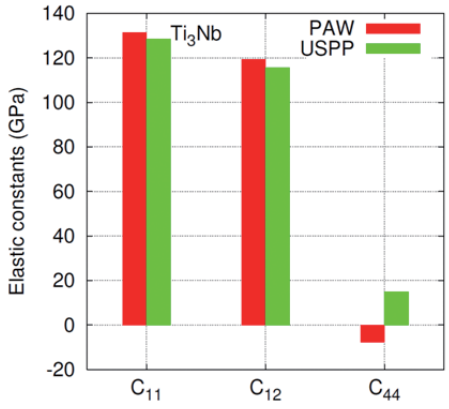

Fig. 2 Elastic constants of $D0_3$-type Ti_3Nb alloy,[4] calculated using the PAW method and compared with the USPP calculations of Ikehata et al.[2]

they are minor effects and will not change the generosity of conclusions.

In the tensile deformation along [100]-direction, original G1-type unit-cell was used as a supercell. In contrast, in the {211}⟨111⟩ shear deformation, we used a supercell where *x*-axis was taken to the shear direction and *z*-axis was taken to the normal direction perpendicular to the shear plane.

Stress-strain curves were obtained by adding the strain to the supercell in small steps. At each deformation step, the crystal structure was fully relaxed such that all lateral stresses vanished. Structural optimization was performed by external optimizer GADGET developed by Bučko et al.[15] GADGET can perform a relaxation of the lattice parameters and the atomic positions simultaneously with several structural degrees of freedom fixed. A high cut-off energy has to be used to ensure a high accuracy of the stress tensors.

The integration in the Brillouin zone (BZ) was performed by the Hermite-Gaussian smearing method with a smearing parameter of 0.2 eV.[16] The sampling *k*-point meshes were properly chosen according to the size and symmetry of the supercells used in the calculations. The very fine *k*-mesh corresponding to $\Delta k < 0.12$ (1/Å) was found to be necessary to calculate the elastic constants and the stress-strain relations.

3. Structure Model for the β-phase of Ti_3Nb Alloys

As we mentioned in the introduction, $D0_3$-type Ti_3Nb was found to be elastically unstable with a negative C_{44}, which means that the $D0_3$ structure is inadequate as a model to predict ideal shear strength. One of the possible reasons for elastic instability may be found when disorder effect of Nb atoms is considered more properly. Therefore, we searched a more reliable structure model for gum-metal approximant by taking into account all the possible arrangement of the four Nb atoms and twelve Ti atoms within the 16-atom supercell containing 2 × 2 × 2 conventional bcc cells. Although there exist 1820 different possible distributions, only the 29 classes of structurally equivalent distributions can be identified as a result of group-theoretical consideration.

After performing structural optimizations and energy evaluations for all of the non-equivalent distributions, G1 structure shown in Fig. 1(b) was found to be the energetically most favorable structure. As shown in Fig. 1(b), G1-type Ti_3Nb is characterized by the chains of Nb atoms along [111]-direction. Although the G1 structure has the space-group symmetry $R\bar{3}m$, the angles between primitive lattice vectors are 89.9º. Namely, the G1 structure is considered to be almost close to the cubic structure. A lattice constant of the G1 structure is a = 6.524 Å for the 2 × 2 × 2 bcc supercell containing 16 atoms. The lattice constant corresponding to the conventional bcc lattice is a_{bcc} = 3.262 Å, which is almost identical with the results for $D0_3$-type Ti_3Nb by Ikehata et al.[2] (3.273 Å) and Sun et al.[17] (3.260 Å). The lattice constant of gum metal measured at the room-temperature is reported to be a_{bcc} = 3.287 Å by Kim et al.[18]

To confirm the elastic stability of the G1 structure, elastic constants were calculated. The results are shown in **Table 1** together with the elastic constants measured by Takesue et al.[19] and by Talling et al.[20,21] for different gum-metal specimens. As obviously seen from Table 1, G1-type Ti_3Nb is elastically stable (i.e., $C_{44}>0$) and its elastic constants C_{44} and C' are found to be very close to those measured by Takesue et al.[19] for single-crystal gum-metal specimens.

Table 1 Elastic constants and tensile and shear moduli (in GPa) calculated for bcc G1-type Ti_3Nb alloys, compared with experimental results measured on gum-metal specimens of slightly different compositions.

Alloy	C_{11}	C_{12}	C_{44}	C'	E_{100}	E_{110}	E_{111}	G_{100}	G_{110}	G_{111}	Reference
Ti_3Nb (G1)	148.8	111.4	37.5	18.7	53.4	83.2	101.8	37.5	18.7	22.4	4
Ti-23Nb-0.7Ta-2Zr-O[a]			28.5-36.6	12.3-17.8	40.0				12.3-13.7	15.1	19
Ti-33Nb-0.7Ta-2Zr-O[a]											
EP[b]	125	93	28	16	49.7	71.8			16	18.7	20
HP[c]	125	90	31	17.5	45.7	65.8			17.5	20.5	20

[a] Composition given in atomic percent.
[b] Produced from elemental powders and cold pressing.
[c] Produced by plasma spraying and hot pressing.

In Table 1, Young's and shear moduli for the principal symmetry directions are also listed since they are important to discuss results shown later. The ideal tensile strength along [100] direction ($\sigma_{\max}^{100}$) and the shear strength along [111] direction ($\tau_{\max}^{111}$) can be estimated empirically from the Young's modulus E_{100} and shear elastic constant G_{111} as follows: $\sigma_{\max}^{100} = 0.08 \times E_{100}$ = 4.3 (4.0) GPa and $\tau_{\max}^{111} = 0.11 \times G_{11}$ = 2.5 (2.3) GPa from the theoretical (experimental) elastic constants.

4. Stabilization of the bcc β Phase by Anharmonic Interactions

The G1-type Ti_3Nb is found to be elastically stable. However, as shown in **Fig. 3**(a), phonon dispersions of the G1 structure calculated at zero temperature in the harmonic approximation show the existence of soft modes over most of the Brillouin zone, which means that the G1 structure is still dynamically unstable at zero temperature.

The dynamical instability of the β phase may be reasonable because more stable martensites such as α', ω, α'' appear at low temperature. To confirm the dynamical stability of the G1 structure at finite temperatures, we performed the phonon calculations with self-consistent phonon theory as implemented in the SCAILD method for temperatures up to 1600 K. Figures 3(b) and (c) show the phonon dispersions at T = 300 K and 600 K, respectively. The results show that the G1-type Ti_3Nb is stabilized already at room-temperature, although the $D0_3$-type Ti_3Nb is found to be dynamically unstable with imaginary phonon modes even at high temperature.[4]

In the next section, we will assume that the G1-type Ti_3Nb binary alloy is a good approximant for the high-temperature bcc phase of gum-metal alloys and then we will present the calculated results of stress-strain curves for tensile and shear deformations in the G1 structure.

5. Prediction of Ideal Strength

5. 1 [100] Uniaxial Loading

To estimate the ideal strength, we calculated stress-strain curves under [100] tensile deformation. The G1-type unit cell of Ti_3Nb shown in Fig. 1(b) was used as a supercell. The integrations in the Brillouin zone were performed with a 8 × 8 × 8 *k*-mesh, which was carefully chosen so as to give sufficiently converged results.

Figures 4(a) and (b) show the energy-strain and stress-strain curves, where we investigated three different conditions. In case 1, tetragonal symmetry is assumed as a guiding symmetry during the tetragonal

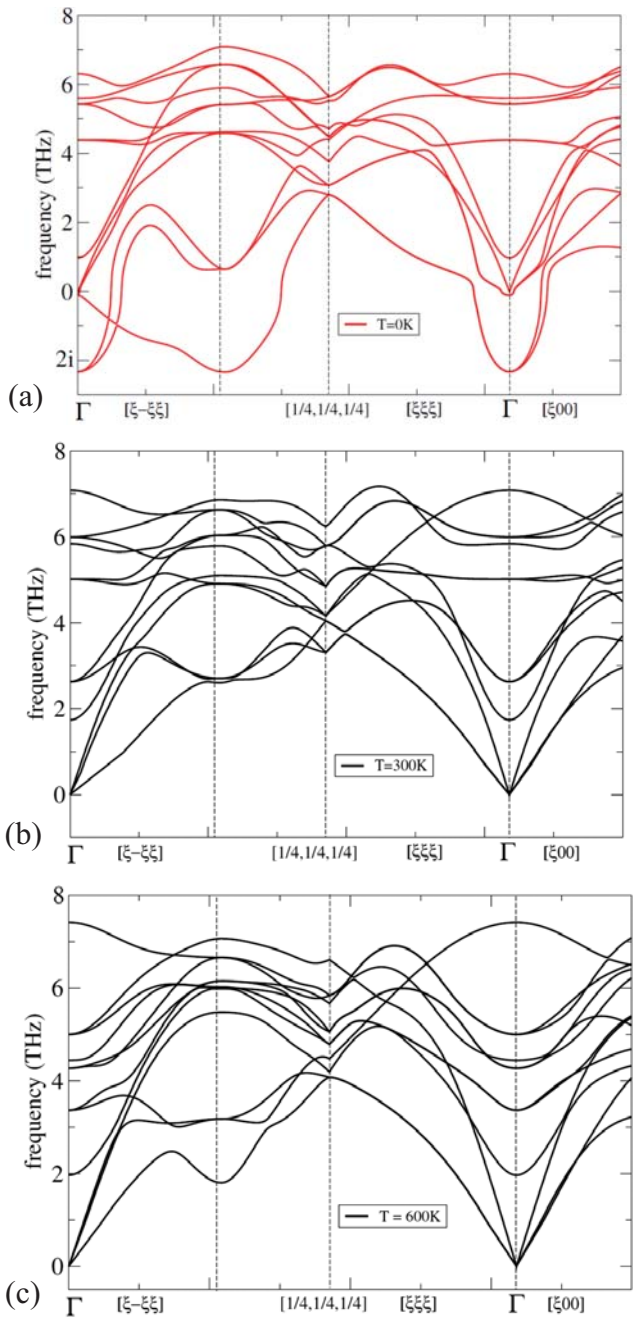

Fig. 3 The phonon dispersions of the Ti_3Nb alloy in the G1 structure, calculated in the harmonic approximation (a) and using self-consistent phonon theory at T = 300 K (b) and T = 600 K (c). The dispersion relations are drawn for the Brillouin zone corresponding to the irreducible four-atom elementary cell.

deformation. On the other hand, in case 2, the symmetry of the cell is initially broken such that the lattice constant b_{SC} and c_{SC} can be different values. In case 3, the angle α_{SC} between lattice vectors $\boldsymbol{b}_{SC}$ = (0, a, 0) and $\boldsymbol{c}_{SC}$ = (0, 0, a) of the supercell is fixed to be 90º during the tensile deformation, where a is the lattice constant of the G1 structure.

From the initial slope of the stress-strain curve we can obtain a tensile modulus of E_{100} = 53.64 GPa, in excellent agreement with the value of 53.4 GPa derived from the elastic constants.

In case 1, stress maximum is reached at the strain of 0.08, where the ideal strength is found to be 2.45 GPa. Case 2 gives almost identical stress-strain relation as case 1 until strain reaches up to 0.06. However, stress is suddenly drop to 1.2 GPa at ε = 0.065, by which ideal strength is limited to be 2.4 GPa in case 2. As can be seen from Fig. 4(b), case 1 and case 2 gives the same results for $0.18 \leq \varepsilon \leq 0.24$, where it is found that angle α_{SC} begins to deviate from 90º, namely, monotonic deformation also begins in addition to the tensile deformation. If α_{SC} is fixed to be 90º during the tensile deformation (case 3), states corresponding to the energy maximum and the local energy minimum, which are stress-free states, are clearly observed at ε = 0.26 and 0.375, respectively, as shown in Fig. 4(a).

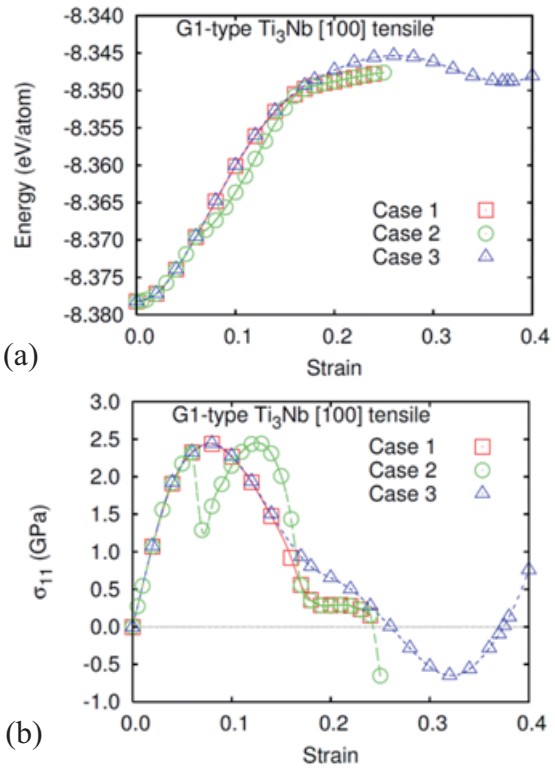

Fig. 4 Variation of the total energy (a) and the stress (b) of G1-type Ti_3Nb under [100] tension as a function of the applied strain, calculated using the cubic unit cell of the G1 structure. The two simulations shown in the diagram (case 1 and case 2) differ by a shear instability at a strain of ε_{11} = 0.06, just before reaching the stress maximum, in case 2. In case 3, calculations are performed with the angle α_{SC} between lattice vectors $\boldsymbol{b}_{SC}$ and $\boldsymbol{c}_{SC}$ of the supercell fixed at 90º.

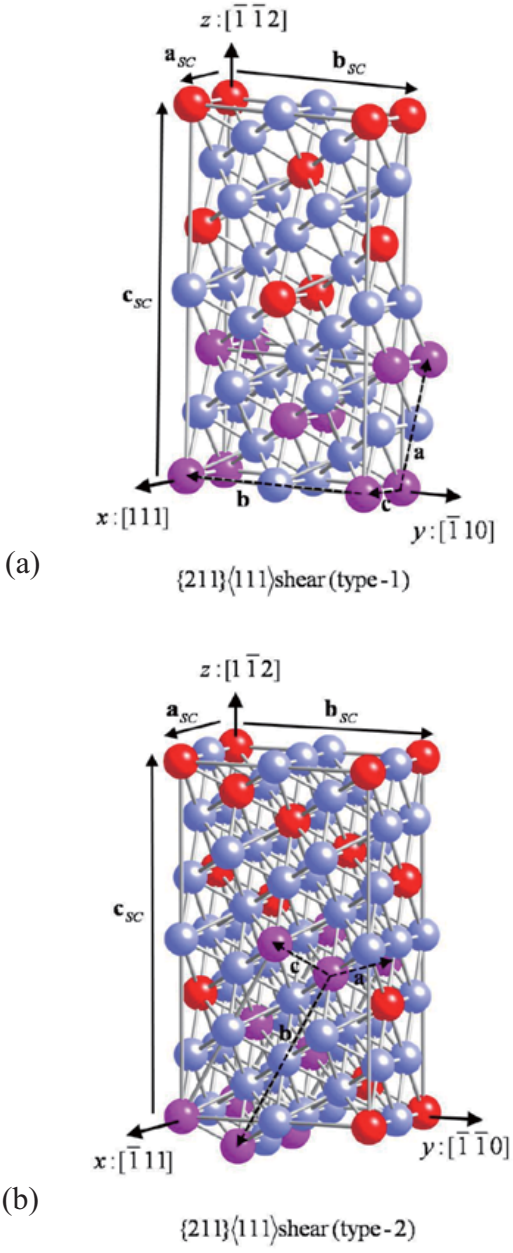

Fig. 5 Supercells used to simulate {211}⟨111⟩ shear deformations, (a) type 1 and (b) type 2. The smaller monoclinic unit cell of the G1 structure has been emphasized.

5. 2 {211}⟨111⟩ Shear Deformation

The {211}⟨111⟩ shear deformation is one of the common slip systems in bcc metals. To investigate the ideal strength in the {211}⟨111⟩ shear deformation, we reconstructed the supercell such that x direction becomes a slip direction and z direction becomes the direction perpendicular to a slip plane. We considered two kind of ⟨111⟩ directions, [111] direction along Nb-Nb chains (type 1) and [$\bar{1}$11] directions along Nb-Ti chains (type 2). The actual supercells used in the present calculations are shown in **Figs. 5**(a) and (b). In type-1 supercell, the undeformed cell has the lattice parameters $a_{SC} = \sqrt{3}a_0 / 4$, $b_{SC} = \sqrt{2}a_0$ and $c_{SC} = \sqrt{6}a_0$, where a_0 is the lattice constant of the G1-type Ti_3Nb. Type-2 supercell has a_{SC} twice as large as the type-1 supercell.

Figure 6 shows the stress-strain curves for {211}⟨111⟩ shear deformation in the G1-type Ti_3Nb, together with the stress-strain curves for {211}⟨111⟩ shear deformation calculated for bcc V, Nb, Ta, Mo and W. The initial slope of the stress-strain curve for G1-type Ti_3Nb gives a shear modulus of $G_{\{211\}\langle 111\rangle} = 24.9$ GPa for both types of supercells. On the other hand, the shear modulus estimated from the calculated elastic constants is $G_{\{211\}\langle 111\rangle} = 22.4$ GPa as already shown in Table1. Both values are in good agreement each other, which means that calculations of the stress-strain curves are performed with high accuracy.

The ideal shear strength (ISS) can be obtained as a maximum value of the stresses. From Fig. 6, it is confirmed that Ti_3Nb indicates significantly small ideal strength compared with the other bcc metals. This is because the elastic softening occurs when the valence electron numbers per atom is around 4.24 featuring the gum-metal composition. In type-1 supercell, the ISS is found to become 1.65 GPa at a strain of 0.12. In contrast, in type-2 supercell, stress-strain curve indicates that shear instability occurs at the strain of 0.12, by which the ISS of the type-2 Ti_3Nb is limited to be 1.45 GPa at the strain of 0.10. The nanopillar experiment[3] showed that the measured strength of gum-metal specimen is 1.7 GPa, which is very close to that predicted for the G1-type Ti_3Nb. Values of the ISS and the shear elastic constants are listed in **Table 2**.

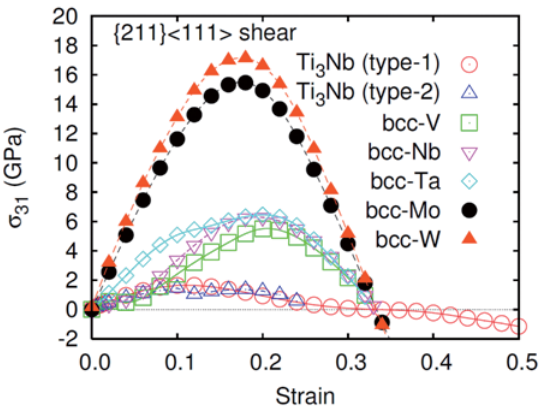

Fig. 6 Comparison of the stress-strain curves of bcc V, Nb, Ta, Mo and W with the G1-type Ti_3Nb alloy under {211}⟨111⟩ shear deformations.

6. Key Mechanisms to Develop Properties of Gum metal

In this section, we would like to discuss key mechanisms to develop properties of gum metal, based on theoretical investigations and experimental observations.

The most important factor is to control a composition of gum metal such that its valence electron numbers per atom becomes around 4.24, by which anomaly of the tetragonal elastic constant occurs. As the result, properties such as a low Young's modulus, elastic softening along a certain direction and lowering of the ideal strength are emerged.

It is also important to keep the bcc structure or the β phase stable since segregation of the low temperature phases such as α', ω, α'' phases increases Young's modulus. Our calculations showed that Nb-Nb chains along [111] direction make the bcc phase elastically stable and also dynamically stable at the room temperature. Namely, inhomogeneous distribution of the Nb atoms are considered to be crucial to stabilize bcc structure under the circumstances where C' becomes very small.

To show the ideal strength, it is necessary to prevent

Table 2 Calculated shear elastic constants G_{111} and ideal shear strength τ_{max} for bcc V, Nb, Ta, Mo, W and G1-type Ti_3Nb.

	G_{111}	τ_{max}
W	141.2	17.1
Mo	132.0	15.5
Ta	53.4	6.46
Nb	31.2	6.28
V	32.7	5.50
Ti_3Nb	22.4	1.45-1.65

moving of dislocations by any kinds of obstacle in addition to the lowering of the ideal strength itself. Unfortunately, we have not yet been able to approach these problems from a microscopic point of view since such problems might depend on the inhomogeneous metallographic structure and effects of impurity atoms. On the other hand, our calculations suggest the existence of Nb-Nb nano clusters. Recent experiments by the X-ray small angle scattering suggest an existence of a certain kind of inhomogeneous structures which is the order of 1 nm in size. In addition, X-ray absorption fine structure analysis of gum metal suggested that Zr-O nano clusters may exist. Therefore, the Nb-Nb and Zr-O nano clusters are expected to play important roles to develop ideal strength, and their quantitative investigations are issues to be addressed in near future.

7. Summary

We investigated stability of the Ti_3Nb by considering all the possible distributions of twelve Ti atoms and four Nb atoms. As the results of structural optimizations, G1-type structure where Nb atoms are located along [111] direction was found to be the most stable. Elastic constants of G1-type Ti_3Nb are in good agreement with those estimated from the experiment, verifying the G1-type structure as a reasonable approximant.

The ideal tensile and shear strength were calculated by the first-principles method for G1-type Ti_3Nb. The ideal tensile strength is found to be 2.4 GPa and the ideal shear strength is found to be 1.45-1.65 GPa, which is much lower than those of bcc simple metals. The predicted shear strength is very close to the experimentally measured strength of gum-metal nanopillars, 1.7 GPa. Thus, it was confirmed both theoretically and experimentally that gum metal is deformed by near ideal strength, which makes the gum metal quite unique to have high strength and ductility simultaneously.

Acknowledgments

Part of this work was a collaboration with P. Lazar, M. Jahnáteck, C. B.-Schenner, M. Stöhr and R. Podloucky at University of Vienna. The authors would like to thank T. Bučko at University of Vienna for providing access to the GADGET structural optimization package.

References

(1) Saito, T., et al., *Science*, Vol. 300 (2003), pp. 464-467.
(2) Ikehata, H., et al., *Phys. Rev. B*, Vol. 70 (2004), 174113.
(3) Withey, E. A., et al., *Acta Mater.*, Vol. 58 (2010), pp. 2652-2665.
(4) Lazar, P., et al., *Phys. Rev. B*, Vol. 84 (2010), 054202.
(5) Blöchl, P. E., *Phys. Rev. B*, Vol. 50 (1994), pp.17953-17979.
(6) Kresse, G. and Joubert, D., *Phys. Rev. B*, Vol. 59 (1999), pp. 1758-1775.
(7) Kresse, G. and Furthmüller, J., *Computat. Mat. Sci.*, Vol. 6 (1996), pp. 15-50.
(8) Kresse, G. and Furthmüller, J., *Phys. Rev. B*, Vol. 54 (1996), pp. 11169-11186.
(9) Perdew, J. P., et al., *Phys. Rev. B*, Vol. 46 (1992), pp. 6671-6687.
(10) Souvatzis, P., et al., *Phys. Rev. Lett.*, Vol. 100 (2008), 095901.
(11) Born, M., *Festschrift der Akad. d. Wissenschaften zu Göttingen, Math. Phys. Klasse* (1951), Springer.
(12) Koehler, T. R., *Phys. Rev. Lett.*, Vol. 17 (1966), pp. 89-91; ibid. Vol. 18 (1967), pp. 654-656.
(13) Choquard, Ph. F., *The Anharmonic Crystal* (1967), W. A. Benjamin.
(14) Cochran, W. and Cowley, R. A., *Handbuch der Physik* (1967), Springer.
(15) Bučko, T., et al., *J. Chem. Phys.*, Vol. 122 (2005), 124508.
(16) Methfessel, M. and Paxton, A. T., *Phys. Rev. B*, Vol. 40 (1989), pp. 3616-3621.
(17) Sun, J., et al., *J. Phys.*: *Condens. Matter*, Vol. 19 (2007), 486215.
(18) Kim, H. Y., et al., *Acta Mater.*, Vol. 54 (2006), pp. 2419-2429.
(19) Takesue, N., et al., *J. Cryst. Growth*, Vol. 311 (2009), pp. 3319-3324.
(20) Talling, R. J., et al., *Scr. Mater.*, Vol. 59 (2008), pp. 669-672.
(21) Talling, R. J., et al., *Scr. Mater.*, Vol. 60 (2009), pp. 1000-1003.

Naoyuki Nagasako
Research Field:
- Computational Physics and its Application to Materials Design

Academic Degree: Dr.Sci.
Academic Societies:
- The Physical Society of Japan
- American Physical Society
- The Japan Institute of Metals

Ryoji Asahi
Research Field:
- Computational Materials Design for Development of Functional Materials such as Thermoelectrics, Photocatlysts, and Photovoltaics

Academic Degree: Ph.D.
Academic Societies:
- The Japan Society of Applied Physics
- American Physical Society
- The Japan Institute of Metals

Awards:
- Advanced Technology Award, the Japan Fine Ceramics Association, 2003
- Corporate Environmental Achievement Award, the American Ceramic Society, 2006
- Technical Development Award, the Chemical Society of Japan, 2006

Jürgen Hafner*
Research Fields:
- Computational Materials Science
- Solid State Theory

Academic Degree: Univ. Prof. Dipl.-Ing. Dr.techn.
Academic Societies:
- Austrian Physical Society
- German Physical Society
- Chemisch-Physikalische Gesellschaft

Awards:
- Ludwig-Boltzmann-Prize of the Austrian Physical Scociety, 1979
- Kardinal-Innitzer-Förderungs-Prize, 1981
- Erwin-Schrödinger-Prize of the Austrian Academy of Sciences, 1995

*Center for Computational Material Science, University of Vienna

